Metrologia 13, 17–28 (1977)

metrologia

NBS-4 and NBS-6: The NBS Primary Frequency Standards*

David J. Glaze, Helmut Hellwig, David W. Allan, and Stephen Jarvis, Jr.
Time and Frequency Division, National Bureau of Standards, Boulder, CO 80302, USA

Received: May 21, 1976, and in revised form: June 24, 1976

Abstract

The NBS primary frequency standard NBS-4 has been operating since January 1973. NBS-5 operated from January 1973 until March 1974. At this time NBS-5 was modified significantly and redesignated NBS-6. The extent and character of these design changes are discussed. NBS-6 operation and evaluation began in March 1975. Results obtained from NBS-4, NBS-5 and NBS-6 are given, along with intercomparisons of some significant parameters.

During 1975, NBS-4 was operated as a clock and a time dispersion of 2.5 ns was obtained for one day. The NBS approach to long term clock operation of the primary standards is discussed. These techniques will probably involve "accuracy servo" methods, and may lead to very accurate clocks with time dispersion less than 1 ns per day.

1. Introduction

NBS-4 and NBS-5 were operated from January 1973 to March 1974 as the NBS primary frequency standards. Subsequently, NBS-4 was the only primary standard used for calibration of the NBS atomic time scale during a period when extensive modification of NBS-5 was underway. These modifications were significant, and the subsequent performance of the modified NBS-5 was very different. Hence, it was decided to redesignate the standard as NBS-6. Stability data and other parameters affected by the modifications were measured and will be reported here. Full accuracy evaluations are underway.

2. The NBS-4 System

As reported earlier [1], development of and modifications to NBS-4 were completed in June 1973. Preliminary evaluations were completed in August 1973, and NBS-4 has been used since that time, together with NBS-5, which was completed in November 1972, for calibration of the NBS atomic time scale. NBS-4 is shown in Figure 1. The beam tube is 1.4 metres long overall, with a Ramsey-cavity interaction length of 52.4 centimetres. The beam tube and vacuum system can be heated to 350°C to aid in outgassing. The system is normally pumped by a single 140 l/s ion pump. Operating pressure is typically 2.7×10^{-7} N/m^2 (2×10^{-9} torr).

Figure 2 gives a general schematic view of the beam optics design of NBS-4. This design utilizes an offset geometry, and as a result, the beam stops and central slit which are used in NBS-5 and NBS-6 are not necessary for filtering very high velocity atoms. In general, atoms

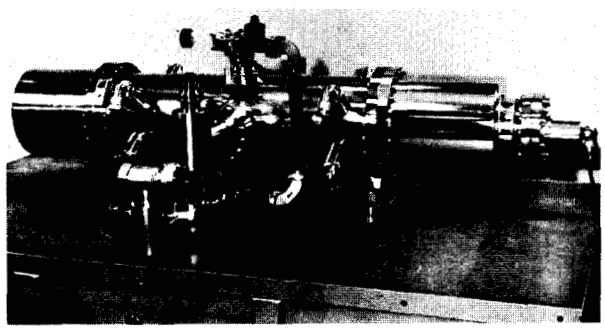

Fig. 1. NBS-4 beam tube. Cesium oven is inside left end bell, while cesium detector is inside right end bell. Low-noise field-effect transistor, operating as source follower is mounted in connector on the right end just outside of vacuum flanges. All electronics systems and vacuum pump are supported by frame below beam tube

* The authors are with Time and Frequency Division, National Bureau of Standards, Boulder, Colo. 80302.

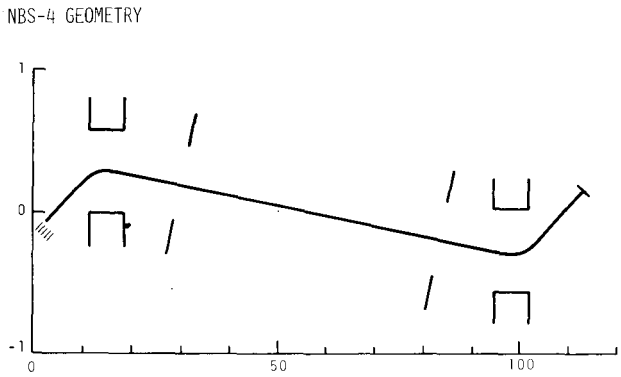

Fig. 2. Schematic drawing of NBS-4 beam tube geometry. Scales are in centimetres. Magnet pole tip locations are represented by unclosed rectangles. Cavity apertures and ionizer ribbon are indicated by straight lines. Collimator openings are represented by group of short lines. Solid line from collimator to ionizer is intended only to show a possible trajectory taken by atoms making transitions

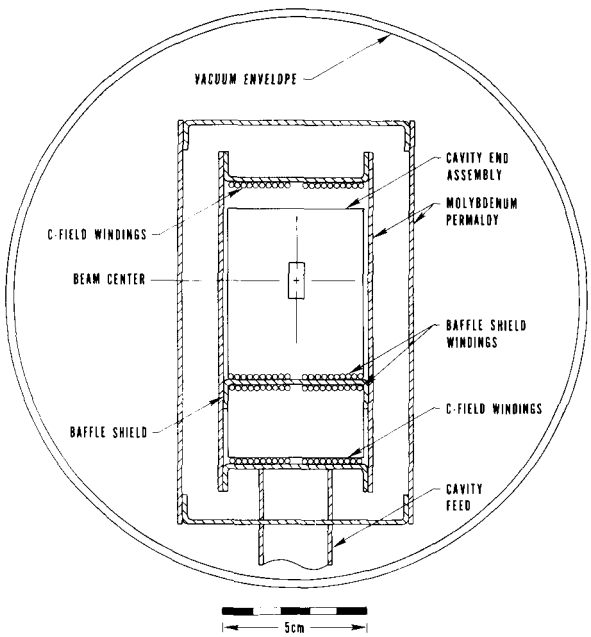

Fig. 3. Cross-section scale drawing of NBS-4 beam tube. Cavity structure and magnetic shields are all electrically insulated from one another except at the cavity feed. There they are joined electrically to one point which is the system ground. Baffle shield and its windings serve to shield beam from opening through which the cavity feed passes. Baffle shield and its windings are approximately 46 cm in length. Inner rectangular molybdenum-permalloy shield and windings define the C-field region of 70 cm in length

reaching the detector may make a transition only in one direction between the ($F = 4, m_F = 0$) and ($F = 3, m_F = 0$) hyperfine levels.

The microwave cavity and magnetic shield structures of NBS-4 are shown schematically in Figure 3. By careful measurement and trimming of the electrical lengths of the cavity arms [2] the phase-angle difference between the two interaction regions of the cavity was adjusted to be significantly less than 1 mrad before assembly of the beam tube. Measurements using the atoms in the cesium beam itself show that the phase-angle difference bias was 0.0 (± 0.06) mrad from January 1973 to May 1975.

The deflection magnets are of a dipole design with a length of 8.9 cm and a gap of about 0.6 cm. The peak flux density at the convex pole tips is about 1.5 T (15 kG). Trimmers are located on the cavity side of each magnet, and are carefully adjusted to assure a smooth transition in field strength as well as field orientation from the high magnetic field of the magnet through the magnetic shield end caps into the shielded cavity region, in order to minimize Majorana transitions. Uncertainties due to the C-field related biases cause a total contribution to inaccuracy of less than 5×10^{-14}. The microwave spectrum (Figure 4) is rechecked infrequently since the C-field parameters are very stable over long periods of time. Indeed, over a month's time the frequency offset of the ($F = 4, m_F = \pm 1$) $\leftrightarrow$ ($F = 3, m_F = \pm 1$) field sensitive transitions, which are used to calibrate the C-field bias, changes only about 2 Hz, out of 42 kHz. This amounts to an error in the frequency of the ($F = 4, m_F = 0$) $\leftrightarrow$ ($F = 3, m_F = 0$) transition of only 1.6×10^{-14}. These changes arise in part from the current source and although very small, they are accounted for in all frequency calibrations. The uncertainty in frequency caused by the use of $\langle H_0 \rangle^2$ for $\langle H_0^2 \rangle$ is conservatively estimated to be $\leq 4 \times 10^{-14}$. This estimate is based on data taken on C-field homogeneity (1) at the time of assembly, from plots of the actual field, and (2) subsequent to assembly, by means of an analysis of the field sensitive transitions, degaussing tests, and linewidth measurements.

It is possible to reverse the beam in NBS-4. However, this can only be done by opening the vacuum chamber and demounting the oven/A magnet assembly and interchanging it with the detector/B magnet assembly. Some rewiring is necessary as well. Since this is a fairly long procedure, and since beam reversal data have been obtained and evaluated from NBS-5 (results were in essential agreement with the pulse method and power-shift method of evaluating cavity-phase shifts [3]), the beam has not been reversed in NBS-4. Also, a beam reversal technique which requires the vacuum system to be opened to the atmospheric environment can lead to errors in the determination of the cavity phase-angle difference bias [4]. Independent accuracy data on NBS-4 were obtained solely by the power-shift method. NBS-4 has some unique features which will permit evaluation of cavity phase-shifts, possibly occurring over the beam cross-section [2, 5, 6]. This is accomplished by movable masks which permit selection of that portion of the opening through which the beam may pass. Atoms may pass through the upper, middle, or lower portions of either opening, or through the entire opening as in frequency standard and clock operation.

The oven cesium charge in NBS-4 is about 0.75 g. The first test of the operating time of this cesium charge occurred in May 1975 when the cesium supply ran out.

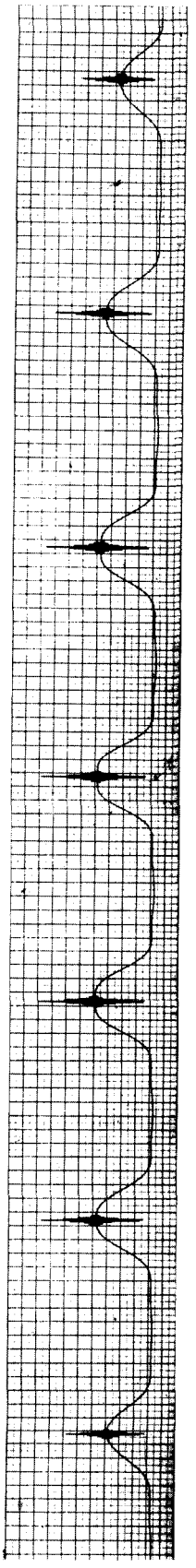

Fig. 4. Microwave spectrum of the σ-transitions ($\Delta F = 1$, $\Delta m_F = 0$) of NBS-4. The center transition ($F = 4$, $m_F = 0$) $\leftrightarrow$ ($F = 3$, $m_F = 0$) is spaced from adjacent transitions by 42.0 kHz corresponding to $H_0 = 4.77$ A/m (60.0 mOe). The width of the central peaks of the Ramsey patterns is about 130 Hz.

The equivalent continuous operating time was about one year. After replacement of the cesium in the oven, NBS-4 was placed in a mode of continuous operation to test performance of the system as a clock. These data and measurements utilizing NBS-4 are presented later in this paper.

3. Some Limitations of NBS-5

The principal limitations of NBS-5, aside from the precision of evaluative experiments, were as follows:

1) In the double beam system [1], cesium accumulation on the ceramic insulators of the detectors caused the leakage resistance of the ion collector to fall below 10^{10} ohms. This reduced the detected beam signal to an unacceptably low level. This contamination persisted in spite of a considerable mass of graphite getter material between the oven and nearby detector. The cesium contamination eventually prevented beam reversal as a routine, operational method. Beam reversal was introduced of course in order to provide the system with the capability of an additional measurement of the cavity phase-difference.

2) The above problem was further aggravated by the fact that the NBS-5 vacuum pumping system [1] inherited from NBS-III was inadequate. This inadequacy caused the pressure along the beam path [pressure estimated to be 1.3×10^{-4} N/m^2 (10^{-6} torr)] to be high enough to cause significant beam scattering. As a result, the oven temperature was raised to 120°C to obtain sufficient signal current; however, this shortened the oven lifetime to about 4 months. The beam scattering effectively filtered out many of the low velocity atoms from the velocity distribution. This, together with the high oven temperature, raised significantly the average velocity of the beam. This increased the velocity dependent biases and increased the Ramsey linewidth to a value of 45 Hz. Pressure changes caused fluctuations in these biases, making accuracy evaluations more difficult by contributing to long-term frequency fluctuations.

3) Because of vacuum system inefficiency, considerable time was required to pump down the system after it had been opened for modification or maintenance.

In spite of the above difficulties, it was possible to achieve a 1σ accuracy of 1.8×10^{-13}. However, in order to achieve accuracies below 1×10^{-13}, it appeared essential to improve the beam tube performance. These considerations led to the major modifications which caused NBS-5 to be changed to the present standard, NBS-6.

4. The NBS-6 Beam Tube

NBS-5, with electronic systems, is shown in Figure 5. NBS-6 is shown in Figure 6. All data from November 1972 to March 1974 were accumulated on NBS-5. Modifications were made during the remainder of 1974 and NBS-6 operation began in March 1975. The extensive

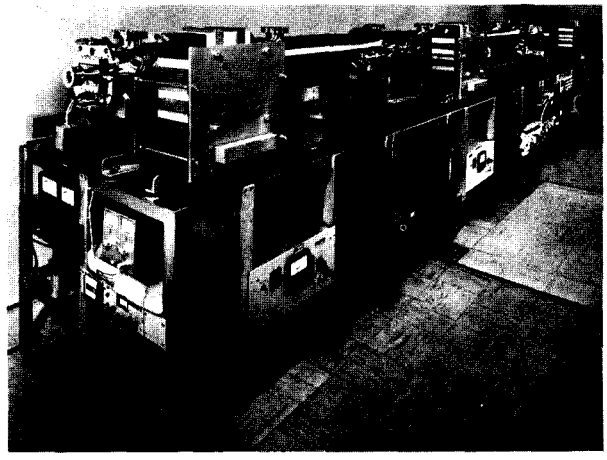

Fig. 5. Pumps shown are 200 l/s. Other electronics systems are mounted below beam tube

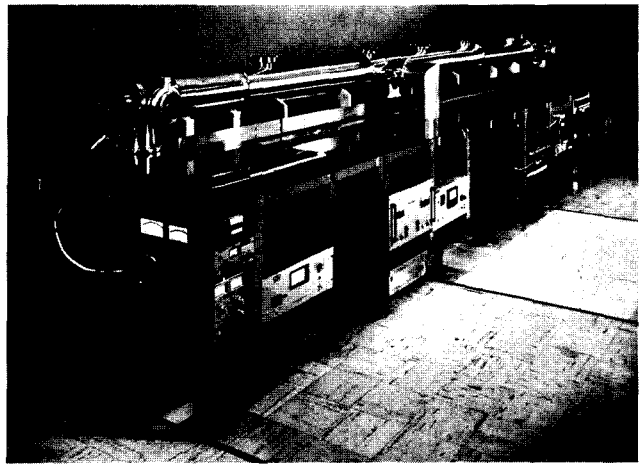

Fig. 6. NBS-6. Solid state electronics systems and new 400 l/s vac-ion pumps are mounted on the frame below the beam tube

modifications were directed towards reduction of the maintenance problems, improvements of the vacuum system, improved beam reversal capability, and the accomplishment of long-term operation of the standard as a clock. Since both the philosophy of operation and the performance were changed significantly, it was decided to redesignate the standard NBS-6.

The most significant changes made were associated with the vacuum system. Larger, more reliable pumps of 400 l/s capacity were added at each end of the beam tube, and pumping conductances to the beam region were significantly improved. The pressure measured at the pumps is now $\leq 1.3 \times 10^{-6}$ N/m^2 (10^{-8} torr). The pressure at the beam position is estimated to be less than 1.3×10^{-5} N/m^2 (10^{-7} torr). These pressures are reduced by more than a factor of 10 compared to those in NBS-5. As a result of these changes, which reduced beam scattering, the Ramsey linewidth was reduced from about 45 Hz in NBS-5 to 26 Hz in NBS-6.

Another improvement to the vacuum system is the addition of a vacuum load-lock system. The vacuum load-lock system, which is an integral part of the beam tube, is shown schematically in Figure 7 with the oven-detector slide in position. A similar arrangement is integrated into the other end of the beam tube so that reversible beam operation is preserved. This arrangement permits a cylinder carrying the oven-detector combination at each end of the beam tube to be removed from the vacuum system without significant increase in pressure. Removal is accomplished by replacement of the oven-detector cylinder with a blank cylinder. Both cylinders carry 0-ring seals. The blank cylinder is placed end to end with the oven-detector cylinder; and then the blank cylinder is pushed slowly, one section at a time, into the vacuum system. This forces out the oven-detector cylinder without causing extraordinarily high pressure in the main vacuum system, providing one stops at each section so that the air trapped between adjacent 0-rings is pumped out to 1.3×10^{-2} N/m^2 (10^{-4} torr) by means of a separate pump port and sorption pump. This method permits changes to be made in the oven-detector system at one end of the beam without significant down time. Indeed, an oven-detector slide can be removed and replaced and operation can be resumed on the same day.

The oven-detector assemblies can be adjusted for beam alignment perpendicular to the beam axis by means of a micrometer. Also, the oven can be aimed at the optimum vertical angle and then locked in position. This adjustment and the alignment in the vertical plane of the beam are used to minimize the beam drop along the path from oven to detector. This gravitational effect can be several millimeters for a beam tube of this length, and proper compensation of trajectory must be used.

The oven and detector are not shown in Figure 7. However, the oven mounts on a plate which fastens into one opening of the slide cylinder, and the detector mounts on a smaller plate into the other opening. There are holes in each plate to permit pumping and entrance or exit of the cesium beam. The holes in the plates are matched by one set of holes on the beam axis in the outer stationary cylinder which is part of the beam tube. Thus when the oven, for example, is aligned with the beam axis, the openings to the detector are completely covered, isolated, and vacuum sealed from the oven. No cesium can reach the detector and contaminate the insulators. The oven and detector are really in two separate chambers inside the slide cylinder. These two chambers are formed by three bulkheads brazed into each oven-detector slide cylinder. One is brazed into the center to prevent cesium transfer from one chamber to the other. Two other bulkheads are brazed into the cylinder to form the ends of the oven and detector chambers. When the oven is turned off, the beam can be reversed by movement of the slides located at each end of the beam tube in such a way that oven and detector are interchanged at each end of the beam tube. The longest delay of about one and one-half hours during this procedure results from the time required for the oven to cool from 89°C to 35°C. Pressure transients are minimal when the slides are operated properly and cause no significant delay. Seals similar to those in the remainder of the vacuum system, rubber 0-rings lubricated with

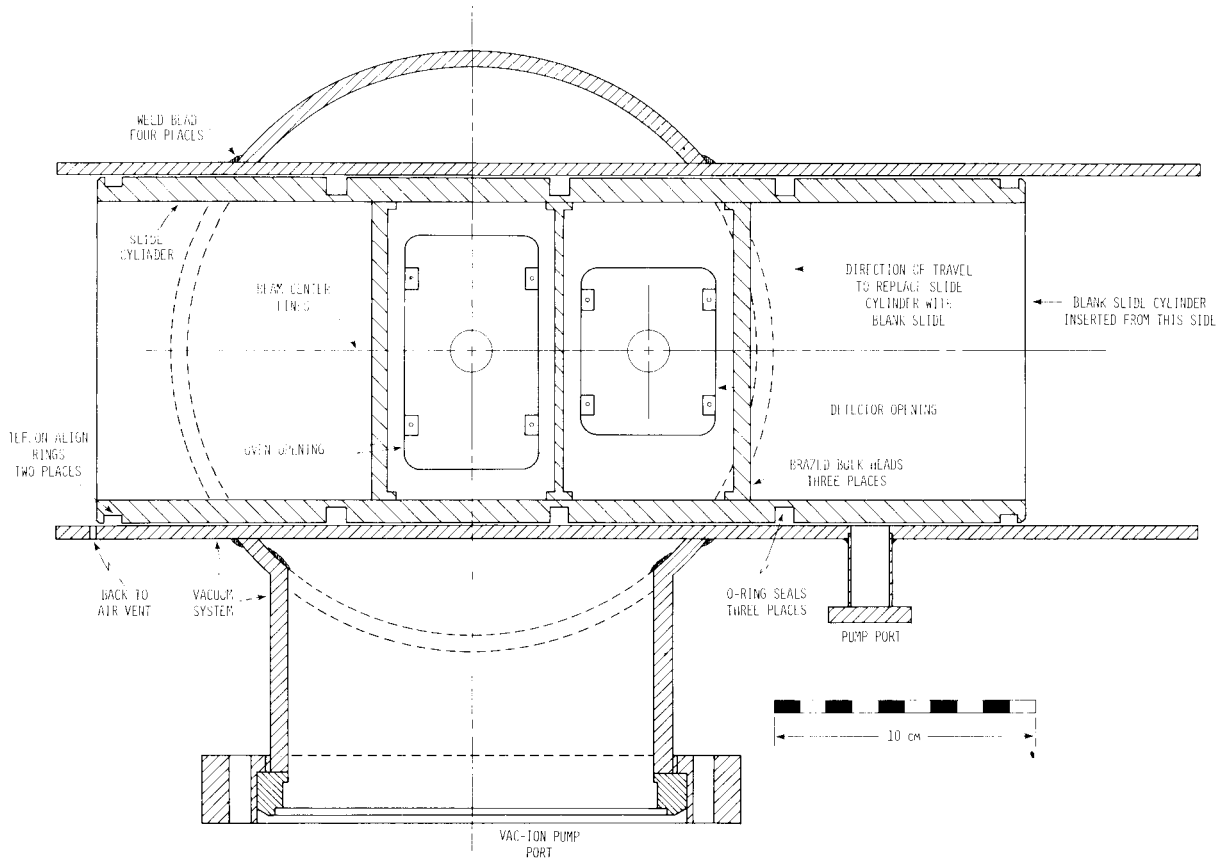

Fig. 7. Cross-section drawing of one of the NBS-6 vacuum load-lock systems. Movable slide cylinder carrying oven and detector is shown in the oven position. The spacing between this cylinder and the outer stationary cylinder, part of the vacuum system, is maintained by two teflon guide rings and the rubber "O"-ring vacuum seals. The rings mount in the five grooves shown. The three rubber vacuum seals isolate the oven and detector chambers and prevent cesium transfer to undesired locations. The oven and detector assemblies are not shown.

To move the slide from the oven position which is shown to the detector position, one simply removes the micrometer positioning assembly (not shown) and moves the slide over to the left to the detector position. The micrometer system is reattached in a predetermined location on the opposite end of the slide cylinder, and the fine adjustment for proper alignment is made with the micrometer. To remove the slide cylinder, one positions a blank cylinder at the right end of the slide cylinder and pushes the blank cylinder into the vacuum system. This is done slowly and in stages so that air trapped between adjacent O-rings is pumped out before one moves to the next section. If the blank cylinder is in the vacuum system and one wishes to install the oven-detector slide, the same procedure is used; the slide to be installed is always inserted from the right to the left

silicone vacuum grease, are employed. This material has caused no problems to date, and system pressures below 1.3×10^{-6} N/m^2 (10^{-8} torr) have been observed. Since O-rings are used, the operator must exercise some care in procedure to avoid both scratches on sealing surfaces and introduction of foreign particles into the system.

The oven can accept ampules filled with 8 grams of cesium. The collimator of the oven is an array of about 500 separate channels producing a beam with rectangular cross-section of 2 mm x 9 mm. With an oven temperature of about 90°C the projected beam flux at the detector is approximately 10^8 atoms/s.

The detector assembly consists of two 90% Pt-10% Ir ionizer ribbons placed side by side. Each ribbon is 0.025 mm in thickness and 4.06 mm in width. The ribbons operate at a temperature of 900°C. No detector failures have occurred in NBS-4, NBS-5, or NBS-6 during almost three years of operation. Because of the relatively high beam intensity (5 pA) and the high purity of the platinum which leads to a total background current for the two ribbons of the order of 1 pA, no mass spectrometer and electron multipler are employed. Instead, two field effect transistors, one for each collector, are mounted in close proximity to the dual detector outside the vacuum system. These transistors have a low gate leakage current of $\leqslant 0.1$ pA and are operated as source-followers. The slightly higher level of background current with two ionizer ribbons does somewhat degrade the short-term stability achievable in NBS-6 with a single detector $[\sigma_y(\tau) = 6 \times 10^{-13} \tau^{-1/2}]$. This high level is rarely needed for frequency calibrations. Therefore, this sacrifice of precision is considered to be acceptable if

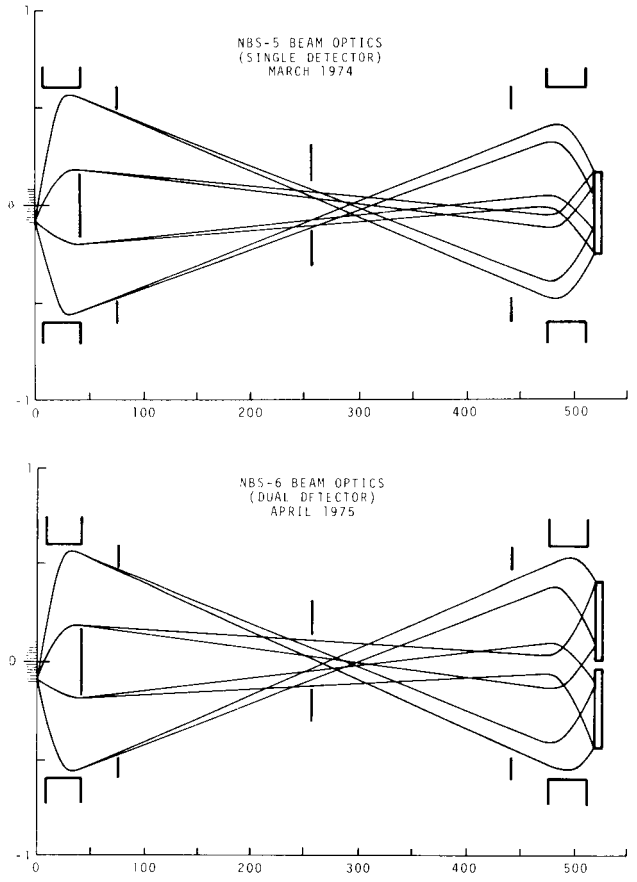

Fig. 8. Beam optics comparisons of NBS-5 and NBS-6. Scales are in centimeters. Cavity and center slit apertures together with beam stops are designated by vertical lines. Magnet gaps are represented by unclosed rectangles, while detectors are shown by closed rectangles. Collimator channel openings are marked by short, horizontal lines. Trajectories shown are only some of the possible ones, but serve to show some of the limiting cases, for atoms making transitions

accuracy can be improved over long periods of time and can be automated, with an accuracy servo to be described.

Figure 8 gives a comparison of the beam optics design of NBS-5 and NBS-6. In contrast to the NBS-5 design utilizing a single detector ribbon centered on the axis, a double detector, consisting of two ribbons, each 4.06 mm in width, placed side by side, is used in NBS-6. The cesium ion currents produced by each ribbon are measured by separate collectors and amplifiers, as explained above. This system, which is presently being evaluated in NBS-6, is designed to permit sensitive measurements to be made simultaneously of the relative velocities of atoms reaching each detector ribbon in the two beams. There is one beam for atoms making a transition from the ($F = 4, m_F = 0$) state to the ($F = 3, m_F = 0$) state and another for the reverse transition. If a change occurs in the relative velocities detected by the two ribbons, the electronics systems can, in principle, detect this change and make a correction. Also, the two beams sample different regions of the microwave cavity apertures; thus, their simultaneous measurement yields information on the distributed cavity-phase difference [6]. This is the basis for the NBS approach to an "Accuracy Servo System" [7] which may permit the combination of clock operation and evaluated long-term accuracy. With this system under development and with the present NBS-4 and NBS-6 reliability, which constitutes a significant improvement with respect to earlier NBS Frequency Standards, long-term clock operation of these standards now appears feasible.

Although the deflecting magnets, cavity, and C-field structures are the same as those in NBS-5 [1], description of those items are included here for completeness. The cavity and magnetic shields for NBS-6 are shown schematically in Figure 9. This basic C-field design is similar to that of NBS-4, although NBS-4 has no Armco shield. The cavity and magnetic shields are located inside the vacuum system in order to insure mechanical stability and to minimize thermal and pressure effects. The interaction length of the Ramsey cavity of NBS-6 is 3.74 m. Adjustments were made, as described in the NBS-4 discussions earlier, to insure that the cavity phase-angle difference was significantly less than 1 mrad at the time of final assembly. This phase-angle difference has not been adjusted since assembly. In subsequent accuracy evaluations, the phase-angle difference was determined to be −0.25 mrad (± 0.15 mrad) [1], using the pulse-excitation method and analysis [3].

The magnetic shield package consists of three separate magnetic shields: two of a box-like structure containing the microwave cavity; the third, outer shield of a cylindrical design. The shields, microwave cavity, and vacuum system are all electrically insulated from one another except at the center of the beam tube where all are joined at one point, the system ground. Figure 10 shows the structure partially disassembled. The typical operating field homogeneity of less than 4.0×10^{-2} A/m (0.5 mOe) peak-to-peak along the tube axis was measured with a field probe after assembly. Two non-inductive heater windings are wound along the length of the rectangular magnetic shield assembly (shown in Fig. 10), one winding on each half of the shield assembly. Thermocouples are located near the resonant cavity end sections and at the center of the cavity. These thermocouples, together with the heater windings, form a system which can be used to heat the cavity uniformly, to prevent cesium deposition inside the cavity, or differentially, one-half with respect to the other, to servo the phase angle difference to zero. This system could be used in the accuracy servo mentioned earlier. In operation the heater system has a long time-constant and requires only a few watts to raise the temperature several K.

One of the two deflection magnets is shown in Figure 11. Each magnet has a length of 35 cm and a gap of 1.2 cm measured at the center. The pole-tip configuration reproduces a two-wire field, and the peak flux density at the pole tip is about 0.93 T (9.3 kG). Trimmers are located on the cavity side of the magnets and are carefully adjusted as described in the discussion of NBS-4.

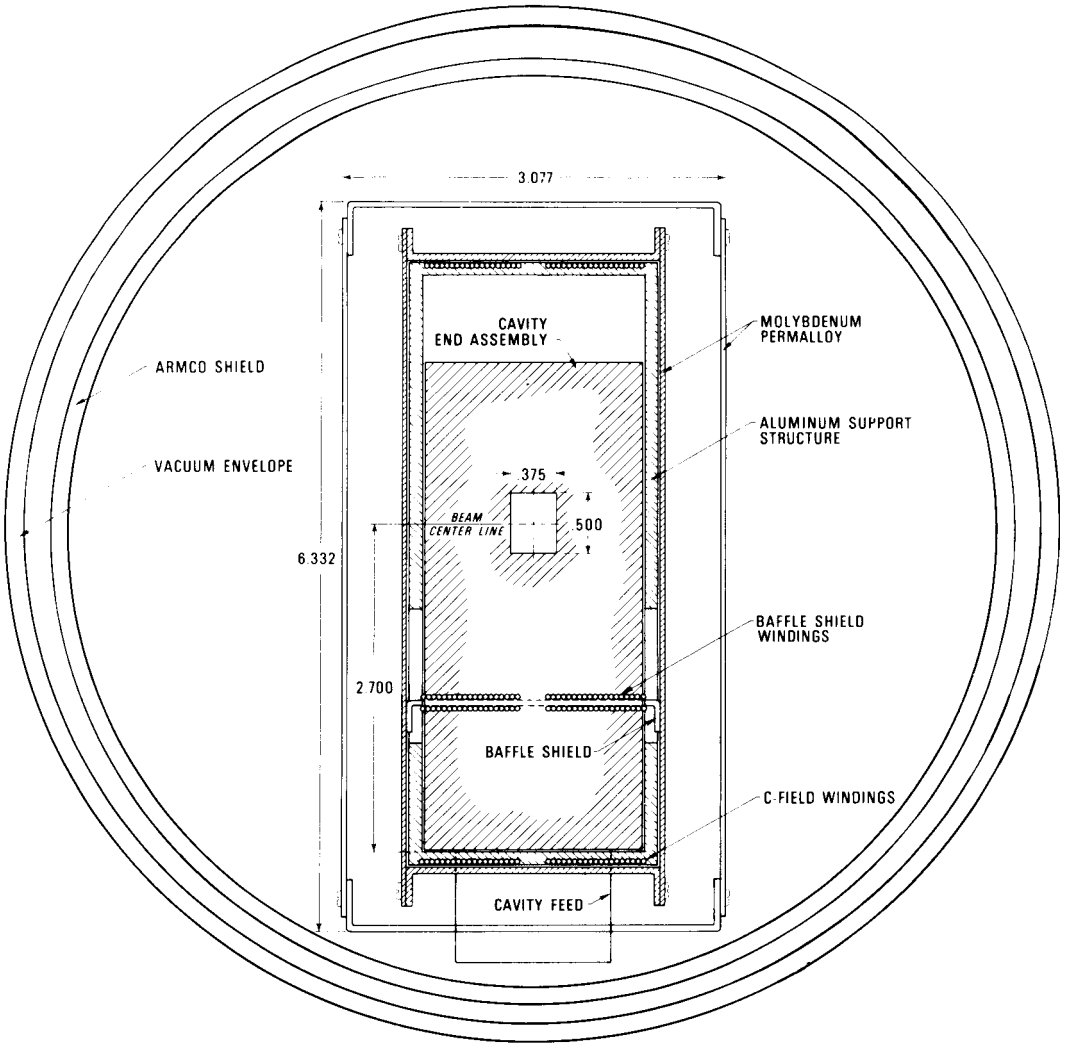

Fig. 9. Cross-section scale drawing of NBS-6 beam tube. Dimensions are in inches. Cavity structure, aluminum support structure, and magnetic shields are all electrically insulated from one another except at the cavity feed. There they are all joined electrically to one point, which is system ground. Baffle shield and its windings serve to shield beam from opening through which the cavity feed passes. Baffle shield and its windings are approximately 76 cm in length. Innermost rectangular molybdenum permalloy shield and windings define the C-field region of 427 cm in length

The beam tube permits an atomic beam to traverse the path through the cavity in either direction. Each end of the beam tube is equipped with identical magnets and oven-detector combinations as described earlier. For beam reversal, the beam stop, shown in Figure 8, can be withdrawn and a second beam stop inserted at the other magnet.

4.1. Operating Parameters and Performance of NBS-6

The operating characteristics of NBS-6 differs in several respects from those of NBS-5. For example, the Ramsey line shapes for the two standards are compared in Figure 12. One can see that the linewidth of 26 Hz for NBS-6 is considerably narrower than that of NBS-5. This improvement is a direct result of more effective filtering of high velocity atoms, reduced scattering of low velocity atoms, and the lower velocity of the beam itself. The reduction of beam scattering of course is due to improved vacuum pumping efficiency already discussed. Also, the shape of the Ramsey pattern of the $(F = 4, m_F = 0) \leftrightarrow (F = 3, m_F = 0)$ transition of NBS-6 is characteristic of a beam having a narrower velocity distribution as compared to the beam in NBS-5. Figure 13 compares the velocity distribution of NBS-5 and NBS-6. Using the pulsed method discussed elsewhere [3], [8], the velocity distributions of Figure 13 were obtained. One can see both the lower velocity spread and the lower absolute velocity of the beam in NBS-6. This lower and more stable velocity should reduce the velocity dependent biases, the principal ones being the cavity phase-angle difference bias and the second order Doppler bias, and may improve significantly the long-term stability of these biases so that clock operation with the primary standard becomes feasible.

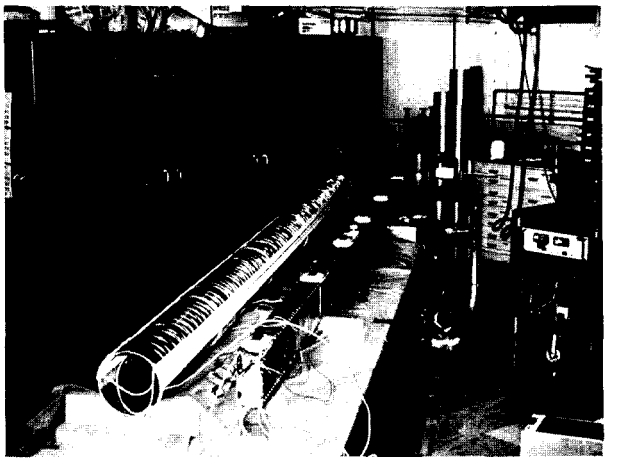

Fig. 10. NBS-6 microwave cavity/magnetic shield package. Cylinder on the left is outer Armco shield. Box structure on the right comprises the two inner shields and contains microwave cavity. (See Fig. 9.) On the cylinder, circumferential windings are for earth-field compensation – used because of required orientation of beam tube. Windings looping through the cylinder are for degaussing. Circumferential windings on box structure are bifilar heater windings described in text

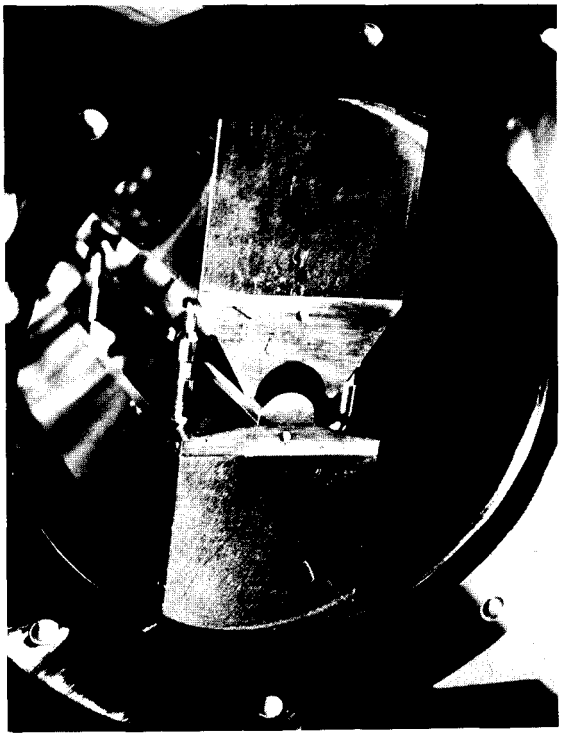

Fig. 11. View of one of NBS-6 dipole magnets. Gap-width 1.2 cm. Pole tips and return ring are soft iron; magnet drivers, between pole tips and return ring, are Alnico-5. Peak flux density in median plane is 0.93 T (9.3 kG)

As a consequence of the decreased beam scattering, the oven temperature has been reduced from 120°C in NBS-5 to 89°C in NBS-6. The reduction of vapor pressure attendant to this temperature reduction is expected to permit about 5 times greater running time for the present 6 g cesium oven charge in NBS-6. The continuous running time at 120°C for NBS-5 was about 4500 hours for the same cesium charge. We therefore expect continuous running time capability for NBS-6 in excess of 2 years per oven.

Since relatively more low velocity atoms traverse NBS-6 than was the case for NBS-5, the width of the beam stop (see Fig. 8) is greater in NBS-6. This gives more effective high velocity filtering of the cesium atoms, and it also causes a narrower velocity distribution and a lower mean velocity (see Fig. 13). The parameter most meaningful for the description of the atomic beam signal-to-noise ratio is the figure of merit [9]. NBS-5 exhibited a fairly stable figure of merit of 150 [1] and a measured short-term stability described by $\sigma_y(\tau) = 8.5 \times 10^{-13}\tau^{-1/2}$, $1\text{ s} \leqslant \tau \leqslant 10^4$ s. From the figure of merit, one expected a $\sigma_y(\tau) = 5.6 \times 10^{-13}\tau^{-1/2}$. The obvious degradation was due both to a small amount of residual phase-noise in the locked oscillator and to the fact that the modulation rate of 18.75 Hz was appreciable compared to the linewidth (see [1]). The measured figure of merit of 100 for the NBS-6 beam tube is lower than that measured for NBS-5 because of the extraordinarily wide dual detector in NBS-6. The added width degrades somewhat the signal-to-noise ratio because relatively more atoms which do not make transitions reach the detector, and because there is more background current from the wider dual-ribbon assembly. In NBS-6, at an oven temperature of 89°C, the measured figure of merit of 100 leads one to expect a $\sigma_y(\tau) = 8.4 \times 10^{-13}\tau^{-1/2}$. The present performance is approximately given by $\sigma_y(\tau) = 2 \times 10^{-12}\tau^{-1/2}$, $1\text{ s} \leqslant \tau \leqslant 10^5$ s. The significant degradation in short term stability is partially due, again, to some phase noise in the locked oscillator. However, the major portion probably comes from the fact that the modulation rate of 18.75 Hz is now even larger compared to the linewidth of 26 Hz. This modulation rate will be reduced in future servo systems. It may be done in new digital, squarewave servo systems now under development [10], which will, at the same time, significantly reduce the effect of oscillator phase noise. The problem of building and proving a phase-modulator with low even-harmonic distortion using the analog servo system [1] would also be removed by a digital servo system.

The microwave spectrum of NBS-6 is shown in Figure 14.

In the upper recording of Figure 14, the Rabi pedestals are shown with their respective Ramsey curves which are at full amplitude. A sweep time of several hours was used for all seven transitions in order to obtain full height for the narrow (30 Hz linewidth) Ramsey curves. These curves appear as vertical lines because the frequency axis is 8.9 kHz per major division. The width of the Rabi pedestals is 20.4 kHz compared

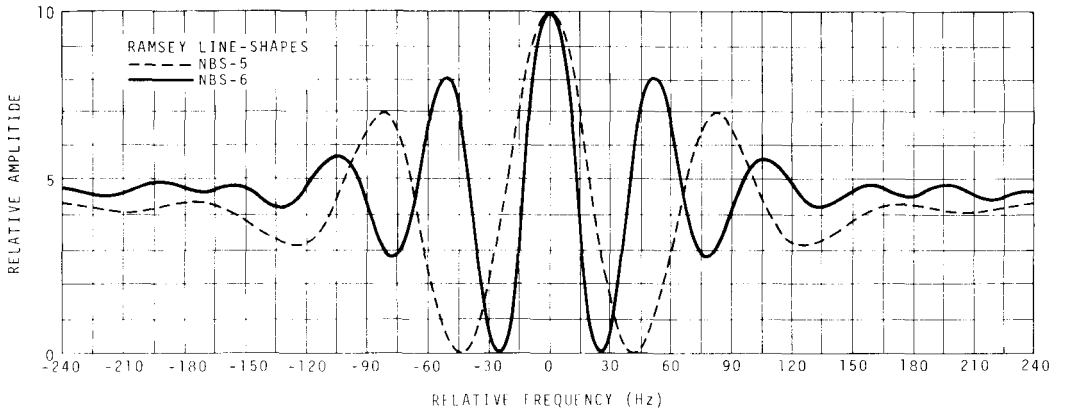

Fig. 12. Ramsey line shapes for NBS-5 and NBS-6. Initial linewidth for NBS-5 was about 30 Hz, but due to vacuum system limitations, this figure became about 45 Hz. Operating value for NBS-6 is 26 Hz and has not shown evidence of deterioration over many months' operation

with 12.0 kHz in NBS-4. This yields a ratio of 1.70. The ratio of the velocities at the peaks of the velocity distributions for the two beams is $(\nu_p$ NBS-6$)/(\nu_p$ NBS-4$) = 1.65$. Thus the broader width of the NBS-6 Rabi pedestal is explained by a higher beam velocity of about 200 m/s in NBS-6. The Ramsey curves are well centered and have good amplitude compared to their respective Rabi pedestals.

In the lower recording of Figure 14, the vertical scale is identical to that in the upper recording. To obtain the lower recording the chart speed was increased to provide an expanded frequency axis (50 Hz per major division) so that the detailed character of all seven Ramsey curves might be examined. One can see that the symmetry and amplitudes of the field dependent Ramsey curves are excellent. The Ramsey linewidths are 30 Hz. One may assume that a linear field inhomogeneity over the beam cross-section is responsible for the reduction (6.5%) of the $(F = 4, m_F = -3) \leftrightarrow (F = 3, m_F = -3)$ Ramsey curve amplitude with respect to its Rabi pedestal as compared to the relative amplitude of the $(F = 4, m_F = 0) \leftrightarrow (F = 3, m_F = 0)$ Ramsey curve to that of its pedestal. In this case, for a Ramsey linewidth of 30 Hz for the $(F = 4, m_F = -3) \leftrightarrow (F = 3, m_F = -3)$ transition, this non-uniformity of field over the beam cross-section is less than 8×10^{-5} A/m (1 μOe) at the operating field value. The corresponding frequency bias would be totally negligible ($<1 \times 10^{-14}$).

However, one must also consider as a limitation on accuracy, the use of $\langle H \rangle^2$ for $\langle H^2 \rangle$. The σ-spectrum recordings of Figure 14 do not show this effect even though they suggest excellent field uniformity. The best measure of this effect is obtained from field graphs at the time of assembly. These graphs were taken with the operating field applied and were obtained by direct measurements of the field. The measurements show an approximately sinusoidal variation of 4×10^{-2} A/m (0.5 mOe) peak-to-peak for the C-field region. The field variation measured would cause less than 1×10^{-14} uncertainty in accuracy due to the use of $\langle H \rangle^2$ for $\langle H^2 \rangle$.

Figure 15 shows stability comparisons for NBS-4 and

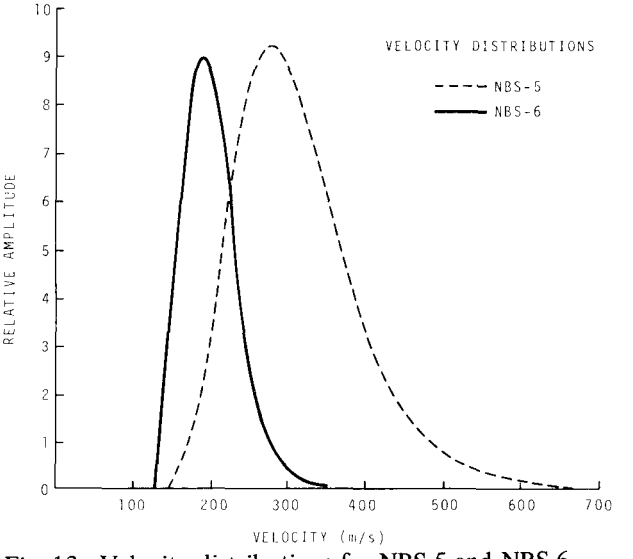

Fig. 13. Velocity distributions for NBS-5 and NBS-6. Data were taken by pulse method [3], [8], and were in agreement with data derived from analysis of the Ramsey line shapes [12]

NBS-5. Figure 16 shows stability comparisons for NBS-4 and NBS-6. Only preliminary data are available at this time concerning the accuracy of NBS-6. Enough data have been taken, however, to permit one to say that the accuracy is at least as good as that reported earlier (1.8×10^{-13}, 1σ) [1]. Also, the bias corrected frequencies of NBS-4, NBS-5, and NBS-6 compared via measurements using the NBS Clock Ensemble and NBS-4, agree to within 1×10^{-13}. The uncertainty of this comparison is estimated to be $\pm 2 \times 10^{-13}$. Because of the improved stability of the velocity distribution, and because of improved evaluative techniques and equipment, one may expect the documented accuracy of the NBS Primary Frequency Standards to improve as more data become available. If it is possible to achieve an accuracy significantly better than 10^{-13}, it will be essential to know the effects of a phase-angle difference which may occur over

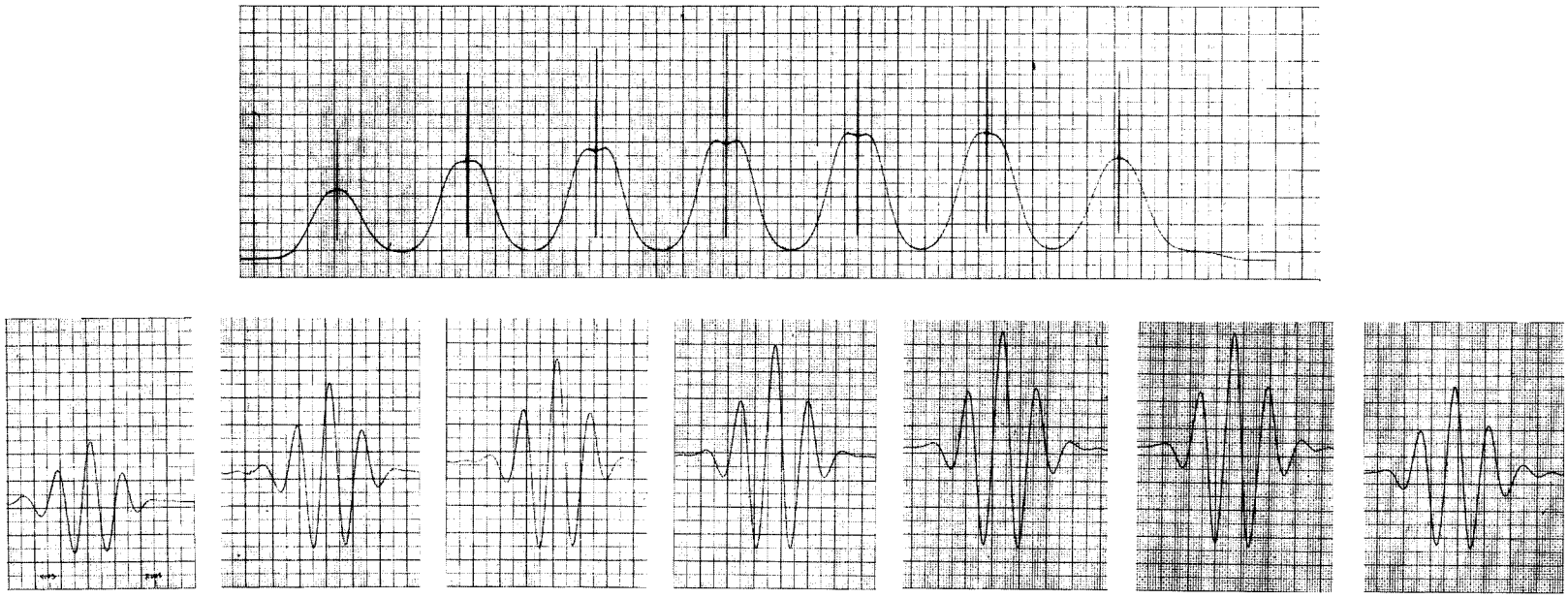

Fig. 14. Microwave spectrum of the σ-transitions ($\Delta F = 1$, $\Delta m_F = 0$) of NBS-6. The microwave power was set to the optimum level for the ($F = 4$, $m_F = 0$) $\leftrightarrow$ ($F = 3$, $m_F = 0$) transition. In the upper recording all seven Rabi pedestals are shown with the respective Ramsey patterns at full amplitude. The sweep speed was slow enough to permit the narrow (30 Hz linewidth) Ramsey patterns to come to full height as the sweep progressed. Frequency axis is 8.9 kHz/major division. The fact that the $\Delta F = 1$, $\Delta m_F = 0$ field dependent Ramsey transitions are so well centered and have good amplitude with respect to their Rabi pedestals, indicate excellent field uniformity. The width of the Rabi pedestals and field uniformity are discussed in the text.

In the lower recording, the vertical scale and sweep rate are exactly the same as in the upper recording. The only difference is that the chart speed was increased to give an expanded frequency axis of 50 Hz per major division so that the character of the Ramsey patterns could be seen

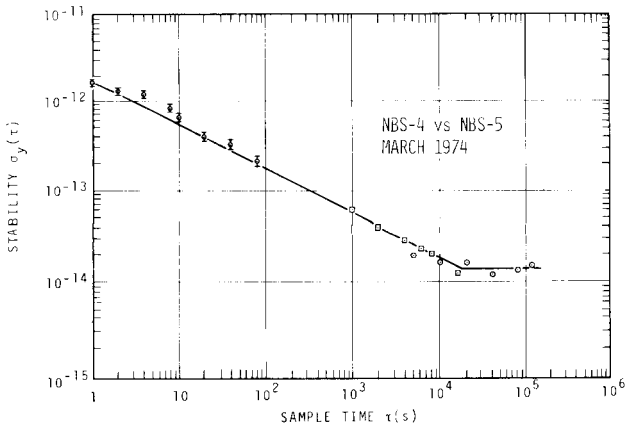

Fig. 15. Frequency stability data from comparisons of NBS-4 and NBS-5

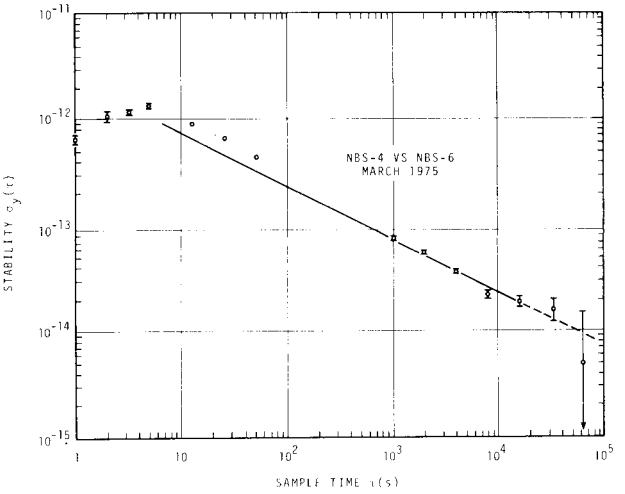

Fig. 16. Frequency stability data from comparisons of NBS-4 and NBS-6

the cross-section of the cavity window. This will be investigated by means of the NBS-4 movable masks discussed earlier, and by theoretical investigation [6].

4.2. Measurements Utilizing the Primary Frequency Standards

During the period in which NBS-6 was being completed, NBS-4 was used for calibrations of the NBS Atomic Time Scale. A plot of AT_0(NBS) with respect to the NBS Primary Frequency Standards since January 1973 is shown in Figure 17. Raw data points are shown as triangles, and weighted data points [11] are shown as circles in Figure 17. Figure 17 also shows the current NBS measurements of the rate of TAI since 1973. These data points are shown as squares. Error bars shown are larger in 1973 than in subsequent years. The earlier data reflect the memory of NBS-III for which the accuracy was only 5×10^{-13}, 1σ. The accuracies of and the calibrations with the primary standards NBS-4 and NBS-5 are combined in an accuracy algorithm [11] in order to obtain a best estimate of the second which yields a combined measurement accuracy of about 1×10^{-13}, 1σ.

Starting on 10 July 1975, NBS-4 was operated as a clock along with the commercial clocks in the NBS Time Scale system. The algorithm employed to generate NBS time assigns weighting factors to each clock depending on each clock's stability characteristics in order to minimize the time dispersion of the time as generated. There are eight clocks in the ensemble and the algorithm arrived at a weight of ~35% for NBS-4 over a one-day

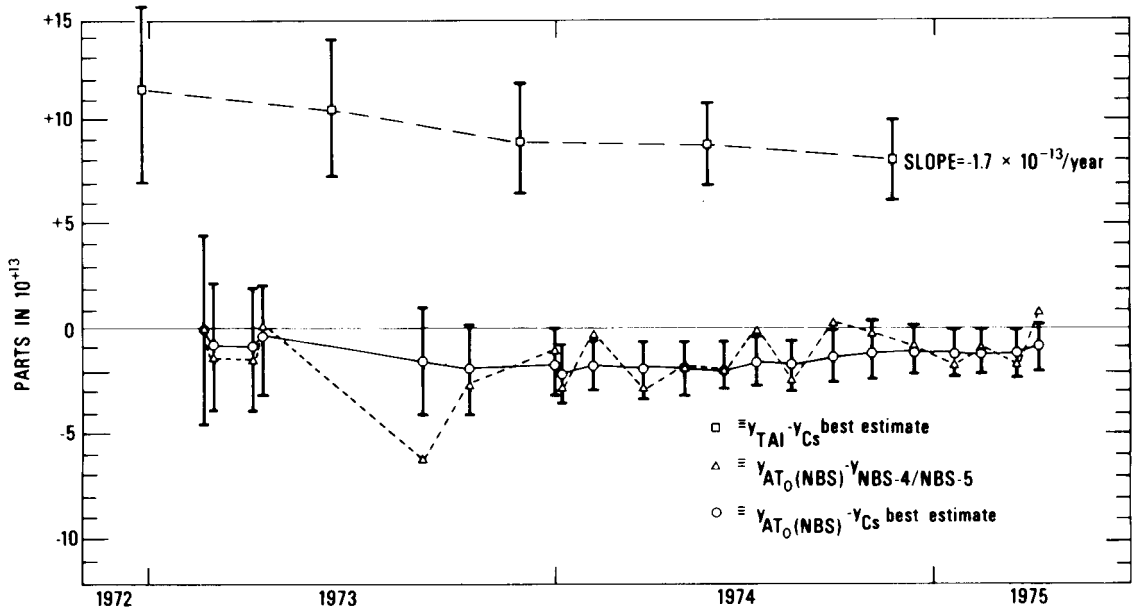

Fig. 17. Frequency calibrations of TAI and AT_0 over two and one-half years using the primary standards NBS-4 and NBS-5

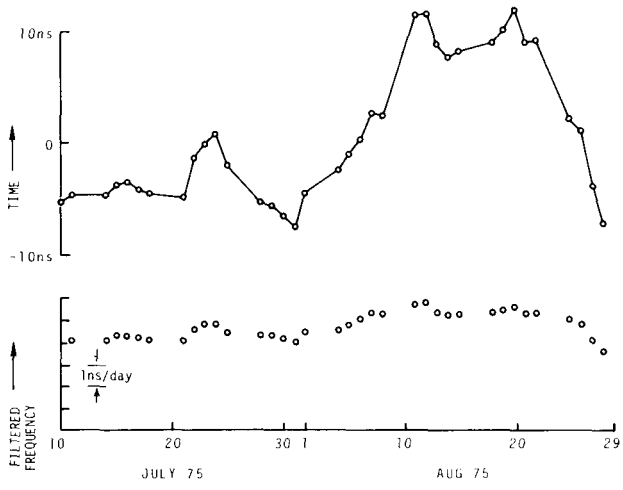

Fig. 18. A plot of the residual time error between NBS-4 and the ensemble of clocks generating the atomic time scale. UTC(NBS) is shown in the upper part of the figure. In the lower part is shown a plot of the residual fractional frequency of NBS-4 vs. UTC(NBS). Taking into account that NBS-4 is a member of the ensemble of clocks, an unbiased estimate of the NBS-4 time dispersion and frequency stability is 2.5 ns per day and $\sigma_y(\tau) \leqslant 2 \times 10^{-14}$ (1 day $\leqslant \tau \leqslant$ 16 days) respectively

time prediction interval and a weight greater than 50% for intervals in excess of a week. Plotted as the upper curve in Figure 18 is the accumulated residual time error between NBS-4 and the time generated by the weighted ensemble, e.g. UTC(NBS). The daily fluctuations plotted need to be amplified by about 1.5 as an unbiased estimate of the true fluctuations due to the fact that NBS-4 is a member of the ensemble. The plot in the lower part of Figure 18 is of the fractional frequency of NBS-4 vs. UTC(NBS); 1 ns/day is about 1.2×10^{-14}. Using these data, one can make an unbiased estimate of the frequency stability for NBS-4 which gives: $\sigma_y(\tau) \leqslant 2 \times 10^{-14}$, 1 day $\leqslant \tau \leqslant$ 16 days; and an estimate of its time dispersion for one day which is 2.5 ns.

5. Conclusion

The reliability of the NBS Primary Frequency Standards has been increased over the past several years because of the efforts of a number of people [1].

The NBS frequency standards are now sufficiently reliable that clock operation of these standards is being initiated with a view towards continuous operation as "super clocks". This concept will of necessity include accuracy servo techniques. The goal is to develop a generation of clocks which will be limited in time error to less than 1 nanosecond per day, and which will maintain this low time dispersion over periods of time from months to years. Many things related to this goal have already been learned as a result of the development and utilization of NBS-4 and NBS-6. The experimental features and capabilities of these standards have not been exhausted, however, and an accuracy better than 10^{-13} appears to be a realistic possibility.

References

1. Glaze, D.J., Hellwig, H., Allan, D.W., Jarvis, S., Jr., Wainwright, A.E.: IEEE Trans. on Instrumentation and Measurement *IM-23*, 489-501 (1974)
2. Lacey, R.F.: Proc. of the 22nd Annual Symposium on Frequency Control, pp. 545-558 (1968)
3. Hellwig, H., Jarvis, S., Jr., Halford, D., Bell, H.E.: Metrologia *9*, 107-112 (1973)
4. Glaze, D.J.: IEEE Trans. on Instrumentation and Measurement *IM-19*, 156-160 (1970)
5. Hellwig, H.: Proc. of the 28th Annual Symposium on Frequency Control, pp. 315-340 (1974)
6. Jarvis, S., Jr.: NBS Technical Note 660 (1975)
7. Hellwig, H., Allan, D.W., Jarvis, S., Jr., Glaze, D.J.: Proc. of the 5th International Conference on Atomic Masses and Fundamental Constants (AMCO-5), Paris, France (1975)
8. Howe, D.A., Bell, H.E., Hellwig, H. DeMarchi, A.: Proc. of the 28th Annual Symposium on Frequency Control, pp. 362-372 (1974)
9. Lacey, R.F., Helgesson, A.L., Holloway, J.H.: Proc. IEEE *54*, 170-176 (1966)
10. Howe, D.A., Salazar, H.F.: Proc. of the 29th Annual Symposium on Frequency Control, pp. 387-393 (1975)
11. Allan, D.W., Hellwig, H., Glaze, D.J.: Metrologia *11*, 133-138 (1975)
12. Jarvis, S., Jr.: Metrologia *10*, 87-98 (1974)